Accurate analytical physical modeling of amorphous InGaZnO thin-film transistors accounting for trapped and free charges

Accurate analytical physical modeling of amorphous InGaZnO thin-film transistors accounting for trapped and free charges

Matteo Ghittorelli, Fabrizio Torricelli, Luigi Colalongo, *Member IEEE*, and Zsolt M. Kovács-Vajna, *Senior Member IEEE*

***Abstract*—A physical-based and analytical drain current model of amorphous Indium Gallium Zinc Oxide (a-IGZO) thin-film transistors (TFTs) is proposed. The model takes into account the combined contribution of both trapped and free charges which move through the a-IGZO film by multiple-trapping-and-release and percolation in conduction band. The model is compared with both measurements of TFTs fabricated on a flexible substrate and numerical simulations. It is accurate in the whole range of a-IGZO TFTs operation. The model requires only physical and geometrical device parameters. The resulting mathematical expressions are suitable for computer-aided design implementation and yield the material physical parameters which are essential for process characterization.**

***Index Terms*—Indium-Gallium-Zinc-Oxide (IGZO), Thin-film transistor (TFT), Computer-aided design (CAD) applications.**

I. Introduction

Among inorganic amorphous oxide semiconductors (AOSs), amorphous Indium Gallium Zinc Oxide (a-IGZO) is a very promising candidate for the next generation thin-film transistors (TFTs) technology, thanks to its large electron mobility ($> 10cm^2/Vs$), optical transparency, mechanical flexibility, low temperature deposition, solution-processability, good device stability and lifetime [1]-[3]. The a-IGZO TFTs have already found application in the backplanes of large-area, high-definition, and flexible displays [4]. In the near future, they are expected to be used also in sensors [5][6], memories [7] and high functionality circuits [8][9]. The development of such applications requires accurate circuit simulation and extensive technology characterization, that, in turn, need physical-based analytical models.

The electrical characteristics of a-IGZO TFTs are strictly related to both the charge transport and the density of trap states (DOS) in the semiconducting layer. The conduction band of a-IGZO is composed of spherical overlapping orbitals. The electron transport path is very efficient thanks to the spherical symmetry, which is less sensitive to the arrangement of atoms [4]. The material disorder leads to potential variations above the mobility band edge and the charge carriers move through the potential barriers thanks to the percolation mechanism [10][11]. However, the spherical overlapping orbitals lead to a small density of trap states, which in a-IGZO is typically 10^{18} cm^{-3} / eV. This is about two orders of magnitude lower than that of amorphous covalent semiconductors. Since in a-IGZO TFTs the total number of trapped states is small ($\sim 10^{18}$ cm^{-3} / eV) [12], it is easy to push the Fermi energy level towards the mobility band edge and attain band-like conduction [13]. This explains the high field-effect mobility values measured in a-IGZO TFTs [4][14]. As a consequence in a-IGZO TFTs a wide energy range in the semiconductor can be spanned by means of the gate voltage V_G and both trapped and free charges have to be accounted for.

In particular, when the transistor works in the weak accumulation regime (small V_G), the Fermi energy level resides within the trapped states and the charge transport is governed by multiple-trapping-and-release (MTR) [15][16]. In a MTR charge transport, the carriers move in delocalized states and interact with the localized states through trapping and thermal release. The amount of trapped charges strictly depends on the energy distribution of the localized states. The DOS shape is usually well approximated by a tail exponential [13][17]-[22] in the energy range 0.2-0.6 eV from the band-edge and by a Gaussian [13][17] or an exponential [18]-[21] function at smaller (deep) energies. As reported in [13][22], the deep states affect only the transistor threshold voltage since they are around $10^{13} \sim 10^{14}$ cm^{-3}. In a-IGZO TFTs such values are achieved when the gate voltage exceeds the flatband voltage of few tens of millivolts and hence the deep states are actually filled.

In strong accumulation regime (large V_G), the Fermi energy level is moving towards the mobility band edge and hence all the trap states become filled. The transport mechanism is now governed by the percolation between the potential barriers and the conductivity is thermally activated [16]. In [13][19], this physical scenario has been validated by comparing a-IGZO TFTs measurements in a wide range of bias conditions and temperatures with numerical simulations.

In the last years, both numerical and analytical compact models for a-IGZO TFTs have been proposed [13][16][18][19][23]-[27]. The numerical models took into account the MTR and percolation transport in the semiconductor, showing that both trapped and free charges have to be considered in a-IGZO transistors. On the other hand, compact models [24]-[27] focused on the accurate description of the transistor electrical characteristics. A physical-based analytical model accounting for the a-IGZO transport physics and able to accurately predict the electrical characteristics of the transistor is still missing.

M. Ghittorelli, F. Torricelli, L. Colalongo, and Z. M. Kovacs are with the Department of Information Engineering, University of Brescia, 25123 - Brescia, Italy. (e-mail: m.ghittorelli@unibs.it)

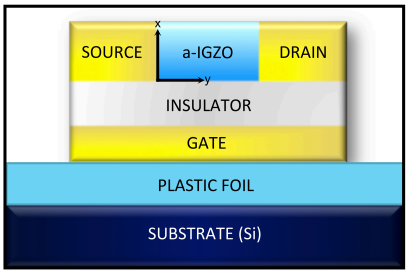

Fig. 1. Schematic cross section of the a-IGZO TFT coplanar structure [26].

In this paper, we propose an analytical model for a-IGZO TFTs that accounts for both MTR and percolation transport. The model includes the contributions of both the trapped and free charges. It is compared with numerical simulations and experimental data collected from transistors fabricated on a flexible substrate. The model is physically based, it enables a detailed discussion of the relative importance of localized and delocalized charges. Furthermore, it can be exploited for physical parameters extraction and, thanks to the analytical formulation, it is suitable for both Computer Aided Design (CAD) implementation and process characterization.

The paper is organized as follow. In Section II, the drain current model is derived. In Section III, the analytical surface potential model is proposed. In Section IV, the analytical model is derived. In Section V the model is validated with the measurements, and the physical parameters are discussed. In Section VI, conclusions are drawn.

II. Drain Current Model

The integral expression of the drain current, based on the Pao-Sah model, is [28]:

$$I_D = \frac{W}{L}\int_{V_S}^{V_D}\int_{V_{ch}}^{\varphi_s}\frac{\sigma(\varphi,V_{ch})}{F_x(\varphi,V_{ch})}d\varphi dV_{ch} \tag{1}$$

where W is the channel width, L is the channel length, V_S and V_D are the source and the drain voltages, respectively, V_{ch} is the channel potential (viz. quasi Fermi potential), φ is the electrostatic potential and φ_s is the surface potential at the insulator-semiconductor interface. It is worth noting that V_{ch} varies along the y-direction while φ depends on both x and y coordinates (Fig. 1).

In order to evaluate the right-hand side of Eq. 1, the conductivity σ and the vertical electric field F_x in the accumulation layer should be expressed as a function of the electrostatic potential φ and of the channel voltage V_{ch}. As reported in [13][22], the shape and the total number of the deep states affects only the threshold voltage, and the density of states can be approximated as a tail exponential function:

$$g_t(E) = \frac{N_t}{k_B T_t}\exp\left(\frac{E-E_c}{k_B T_t}\right) \tag{2}$$

where N_t is the total number of localized states, T_t is the characteristic temperature of the tail states, k_B is the Boltzmann constant, E_c is the conduction-band edge, which is assumed as the energy reference: $g_t(E) = 0$ at $E > E_c$. The conductivity of a-IGZO semiconductor has to account for both MTR and percolation transport mechanisms and reads [16]:

$$\sigma = \sigma_0 \exp\left(\frac{\varphi - V_{ch}}{V_f}\right) \tag{3}$$

where $\sigma_0 = q\mu_B N_f \exp[\Delta E_{Fi}/(k_B T)]$, $V_f = k_B T/q$, $\mu_B = \mu_0 \exp[-\phi_{B0}/V_f + \sigma_B^2/(2V_f^2)]$, is the band mobility μ_0 modulated by a percolation term [16], N_f is the number of states per unit volume in the transport band, and $\Delta E_{Fi} = E_{gap}/2$. The electric field in the x-direction $F_x(\varphi, V_{ch})$, calculated by means of the Poisson equation is $\nabla^2\varphi = -(\partial F_x/\partial x + \partial F_y/\partial y)$ and assuming the gradual channel approximation (i.e. $F_x \gg F_y$) [29], reads:

$$F_x(\varphi,V_{ch}) = \sqrt{\frac{2q}{\epsilon_s}\int_{V_{ch}}^{\varphi} n(\varphi',V_{ch})d\varphi'} \tag{4}$$

$$\simeq \sqrt{k_f e^{\frac{\varphi-V_{ch}}{V_f}} + k_t e^{\frac{\varphi-V_{ch}}{V_t}}} \tag{5}$$

where ϵ_s is the a-IGZO semiconductor permittivity, $n = n_t + n_f$ is the total charge carrier concentration, n_t is the trapped charge concentration, n_f is the free charge concentration, $k_f = 2qN_fV_f/\epsilon_s$, $V_t = k_B T_t/q$, and $k_t = 2\pi N_t k_B T/[\epsilon_s \sin(\pi T/T_t)]$.

Replacing Eq. 3 and Eq. 5 in Eq. 1, the resulting equation hampers any analytical solution [29]. We approximate the inner integral of Eq. 1 as:

$$\int_{V_{ch}}^{\varphi_s}\frac{\sigma_0 e^{\frac{\varphi_s-V_{ch}}{V_f}}}{\sqrt{k_f e^{\frac{\varphi_s-V_{ch}}{V_f}} + k_t e^{\frac{\varphi_s-V_{ch}}{V_t}}}}d\varphi \simeq \frac{\sigma_0 e^{\frac{\varphi_s-V_{ch}}{V_f}}}{\sqrt{k_f\left(\frac{1}{2V_f}\right)^2 e^{\frac{\varphi_s-V_{ch}}{V_f}} + k_t\left(\frac{1}{V_f}-\frac{1}{2V_t}\right)^2 e^{\frac{\varphi_s-V_{ch}}{V_t}}}} \tag{6}$$

Eq. 6 is a continuous function that accurately approximates the integral in the whole energy range and not only in the asymptotic regions (subthreshold and strong accumulation) as in the conventional approaches used for amorphous silicon [30]. The idea is to combine the two asymptotic behaviours of the integrated function. In the weak accumulation regime the free charge contribution is negligible and hence only the trapped charge contribution can be taken into account and Eq. 6 would result: $\sigma_0 e^{\frac{\varphi_s-V_{ch}}{V_f}} / \left[\sqrt{k_t}\left(\frac{1}{V_f}-\frac{1}{2V_t}\right)e^{\frac{\varphi_s-V_{ch}}{2V_t}}\right]$. In the strong accumulation regime the trapped charge contribution is negligible and hence only the free charge contribution can to be taken into account and Eq. 6 would result: $\sigma_0 e^{\frac{\varphi_s-V_{ch}}{V_f}} / \left[\sqrt{k_f}\left(\frac{1}{2V_f}\right)e^{\frac{\varphi_s-V_{ch}}{2V_f}}\right]$. In order to account for also the transition regime between weak accumulation and strong accumulation, we unify these two expressions by means of Eq. 6.

Fig. 2 shows the comparison between the drain current (Eq. 1) calculated with the proposed approximation (Eq. 6) and its exact numerical solution as a function of the gate voltage V_G and of the correlation index (T_t/T). The latter is a synthetic

parameter that ranging from 1 to 3 spans the whole space of the DOS measured in a-IGZO [13], [17]-[22]. As the correlation index decreases, the width of the trapped density of states also decreases, resulting in a steeper subthreshold slope. As shown in the inset of Fig. 2 the proposed approximation is very accurate (max. error $< 4\%$) in the whole range of gate voltages and DOS parameters. It is worth noting that the case of correlation index (T_t/T) less than one, i.e. $T_t < T$ (shallow tail states), is very different from that of $T_t > T$ (wide tail states). When $T_t < T$ the trapping would be insignificant and the trap states have to be extracted from the low temperature measurements [31]. The proposed model holds in both cases $T_t > T$ and $T_t < T$. In the case of shallow tail states $T_t < T$ the trapped charges can be neglected letting $k_t = 0$.

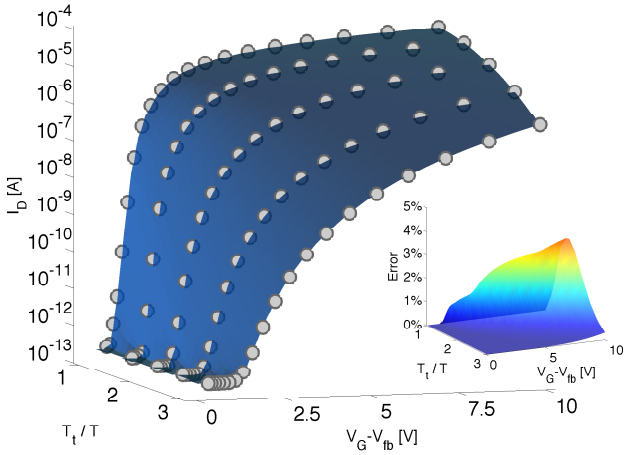

Fig. 2. Main Panel: Transfer characteristics of a-IGZO TFT at $V_D = 1$V as a function of T_t/T. Grey circles are the numerical solution of Eq. 1, blue surface is the numerical solution of Eq. 1 with the analytical approximation proposed in Eq. 6. Inset: percentage error given by the approximation. The physical parameters are listed in Tab. I.

By applying the Gauss law at the insulator-semiconductor interface one obtains:

$$\frac{C_i}{\epsilon_s}(V_G - V_{fb} - \varphi_s) = F_x(\varphi_s, V_{ch}) \tag{7}$$

where C_i is the gate capacitance per unit area, V_G and V_{fb} are the gate and the flatband voltages, respectively. Substituting Eq. 5 in Eq. 7, and after straightforward manipulations one obtains:

$$dV_{ch} = -1 - \frac{\epsilon_s}{2C_i}\frac{\frac{k_t}{V_t}e^{\frac{\varphi_s - V_{ch}}{V_t}} + \frac{k_f}{V_f}e^{\frac{\varphi_s - V_{ch}}{V_f}}}{F_x(\varphi_s, V_{ch})}d(\varphi_s - V_{ch}) \tag{8}$$

The first term at the right hand side can be neglected since the gate voltage is few tens of millivolts larger than the flatband voltage. Replacing Eq. 8 in Eq. 1 and changing the integration variable from V_{ch} to $\psi = \varphi_s - V_{ch}$ the drain current turns out to be:

$$I_D = \frac{W}{L}\beta\int_{\psi_D}^{\psi_S}\frac{\frac{k_f}{V_f}e^{\frac{\psi}{V_f}} + \frac{k_t}{V_t}e^{\frac{\psi}{V_t}}}{\sqrt{a + b\,e^{\frac{\psi}{V_t}-\frac{\psi}{V_f}} + c\,e^{\frac{\psi}{V_t}-\frac{\psi}{V_f}}}}d\psi \tag{9}$$

where $\psi_S = \varphi_{sS} - V_S$, $\psi_D = \varphi_{sD} - V_D$, φ_{sS} and φ_{sD} are the surface potential calculated at the source and the drain contacts, respectively, and,

$$\beta = \frac{\epsilon_s\sigma_0}{2C_i} \quad ; \quad a = \frac{k_f^2}{4V_f^2} \quad ; \quad c = \left(\frac{k_t}{V_f} - \frac{k_t}{2V_t}\right)^2$$

$$b = k_f k_t\left(\frac{3}{2V_f^2} - \frac{1}{V_f V_t} + \frac{1}{4V_t^2}\right)$$

Finally, using the same approximation proposed in Eq. 6, the drain current reads:

$$I_D = [I_{dF}(\psi_S) + I_{dT}(\psi_S)] - [I_{dF}(\psi_D) + I_{dT}(\psi_D)] \tag{10}$$

where I_{dF} and I_{dT} are defined as follow:

$$I_{dF}(\psi) = \frac{W}{L}\beta\frac{\frac{k_f}{V_f}e^{\frac{\psi}{V_f}}}{\sqrt{A_F + B_F\,e^{\frac{\psi}{V_t}-\frac{\psi}{V_f}} + C_F\,e^{\frac{2\psi}{V_t}-\frac{2\psi}{V_f}}}} \tag{11}$$

$$I_{dT}(\psi) = \frac{W}{L}\beta\frac{\frac{k_t}{V_t}e^{\frac{\psi}{V_t}}}{\sqrt{A_T + B_T\,e^{\frac{\psi}{V_t}-\frac{\psi}{V_f}} + C_T\,e^{\frac{2\psi}{V_t}-\frac{2\psi}{V_f}}}} \tag{12}$$

and

$$A_F = \frac{a}{V_f^2};\ B_F = b\left(\frac{3}{2V_f} - \frac{1}{2V_t}\right)^2;\ C_F = c\left(\frac{2}{V_f} - \frac{1}{V_t}\right)^2$$

$$A_T = \frac{a}{V_t^2};\ B_T = \frac{b}{4}\left(\frac{1}{V_f} + \frac{1}{V_t}\right)^2;\ C_T = \frac{c}{V_f^2}$$

Eqs. 10, 11, and 12 give the a-IGZO drain current as a function of the band bending calculated at the source and the drain contact (viz. ψ_S and ψ_D), the applied voltages (V_G,V_S, and V_D) and the a-IGZO TFT physical and geometrical parameters. In particular, I_{dF} mainly depends on the free charges while I_{dT} mainly depends on the trapped charges. As shown in Fig. 3, in weak accumulation (i.e. at small V_G), I_{dF} is negligible and the drain current is basically defined by the trapped charges I_{dT}. At large V_G, I_{dT} is almost constant and the drain current is basically defined by free charges I_{dF}.

The proposed model extends our previous work [28] because (i) it accounts for both multiple trapping and release and percolation charge transport, and (ii) it includes the contributions of both trapped and free charges induced by the vertical electric field. The model in [28] (Eqs. 17-18) can be straightforwardly derived from the model here proposed (Eqs. 10-12) by letting $\mu_B = \mu_0$ in Eq. 3 (no percolation), and assuming that the trapped charge is much greater than the free charge (i.e. $k_f = 0$ in Eq. 5 only).

III. Surface Potential Model

The drain current (Eq. 10) is an analytical function of the band bending at the source and the drain contact (i.e. ψ_S and ψ_D) that in turn are functions of the external voltages (V_G,V_S, and V_D). The surface potential and eventually the band bending ($\psi = \varphi_s - V_{ch}$) can be calculated by replacing Eq. 5 in Eq. 7:

$$\frac{C_i^2}{\epsilon_s^2}(V_G - V_{fb} - V_{ch} - \psi)^2 = k_f\exp\left(\frac{\psi}{V_f}\right) + k_t\exp\left(\frac{\psi}{V_t}\right) \tag{13}$$

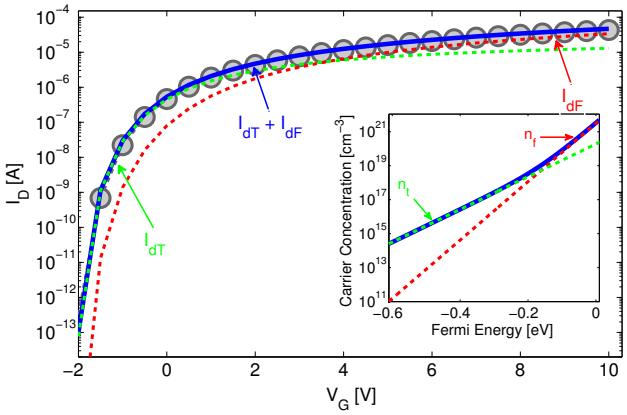

Fig. 3. Main Panel: Transfer characteristic at $V_D = 1$V. Circles are the numerical solution of Eq. 1, full line is the analytical model (Eq. 10). The green dashed line is the current accounting for only the trapped charges I_{dT} (Eq. 12) while the red dashed line is the current accounting for only the free charges I_{dF} (Eq. 11). Inset: charge carrier concentration as a function of the Fermi energy (referring to E_C). The full line is the total charge n, the green dashed line is the trapped charge n_t and the red dashed line is the free charge n_f. The a-IGZO TFTs parameters are listed in Tab. I.

Unfortunately, Eq. 13 is an implicit equation and it can be solved only by numerical iterations. To develop a fully analytical model, an explicit expression of the band bending is required.

In order to work out an accurate analytical approximation we calculate an initial guess solution of the band bending ψ_0 and than we use a single iteration of Newton-Raphson method:

$$\psi = \psi_0 - \frac{f(\psi_0)}{f'(\psi_0)} \tag{14}$$

An accurate initial guess ψ_0 is given by the band bending accounting for only the trapped charge and it reads:

$$\frac{C_i^2}{\epsilon_s^2}(V_G - V_{fb} - V_{ch} - \psi_0)^2 = k_t \exp\left(\frac{\psi_0}{V_t}\right) \tag{15}$$

where

$$\psi_0 = V_t \log\left[\frac{C_i^2}{\epsilon_s^2}\frac{(V_G - V_{fb} - V_{ch} - \psi_0)^2}{k_t}\right] \tag{16}$$

To ensure the quadratic rate of convergence of the solution (viz. high accuracy), we apply the $\log(.)$ function to both sides of Eq. 7 and hence $f(\psi)$ reads:

$$f(\psi) = \log\left[\frac{C_i^2}{\epsilon_s^2}(V_G - V_{fb} - V_{ch} - \psi)^2\right] - \log\left[F_x^2(\psi)\right] \tag{17}$$

and its first derivative, $f'(\psi)$, reads:

$$f'(\psi) = -\frac{\frac{k_t}{V_t}e^{\frac{\psi}{V_t}} + \frac{k_f}{V_f}e^{\frac{\psi}{V_f}}}{F_x^2(\psi)} - \frac{2}{V_G - V_{fb} - V_{ch} - \psi} \tag{18}$$

The second term of Eq. 18 is negligible when the a-IGZO TFT works in above threshold regime ($V_G - V_{fb} > V_{ch}$) and hence, Eq. 18 is approximated as:

$$f'(\psi) \simeq -\frac{\frac{k_t}{V_t}e^{\frac{\psi}{V_t}} + \frac{k_f}{V_f}e^{\frac{\psi}{V_f}}}{F_x^2(\psi)} \tag{19}$$

Substituting Eq. 16 in Eqs. 17 and 19, results:

$$f(\psi_0) = -\log\left\{1 + \frac{k_f}{k_t^{\frac{T_t}{T}}}\left[\frac{C_i}{\epsilon_s}(V_G - V_{fb} - V_{ch} - \psi_0)\right]^{\frac{T_t}{T}-1}\right\} \tag{20}$$

and

$$f'(\psi_0) \simeq \frac{\frac{1}{V_t} + \frac{1}{V_f}\frac{k_f}{(k_t)^{\frac{T_t}{T}}}\left[\frac{C_i}{\epsilon_s}(V_G - V_{fb} - V_{ch} - \psi_0)\right]^{\frac{T_t}{T}-1}}{1 + \frac{k_f}{(k_t)^{\frac{T_t}{T}}}\left[\frac{C_i}{\epsilon_s}(V_G - V_{fb} - V_{ch} - \psi_0)\right]^{\frac{T_t}{T}-1}} \tag{21}$$

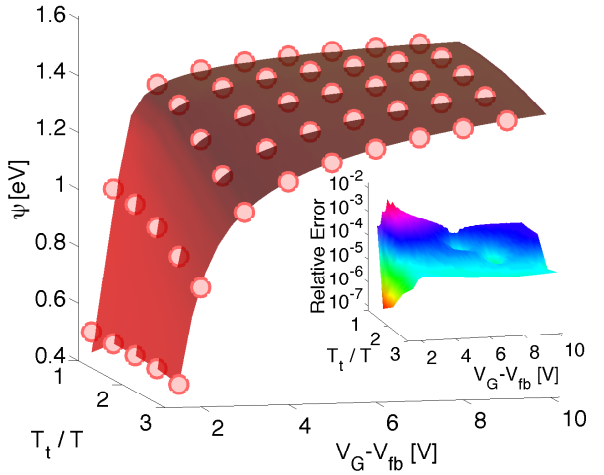

Fig. 4. Main Panel: Band bending as a function of $V_G - V_{fb}$ and correlation index (T_t/T) at $V_{ch} = 1$V. Circles are the numerical solution of Eq. 13, and the surface is the approximate solution Eq. 22. Inset: Relative error of the analytical approximation. Parameters are listed in Tab. I.

Finally, replacing Eqs. 16, 20, and 21 in Eq. 14 one obtains an analytical expression for the band banding:

$$\psi = V_t \log\left[\frac{C_i^2}{\epsilon_s^2}\frac{k_\psi(\psi_0)(V_G - V_{fb} - V_{ch} - \psi_0)^2}{k_t}\right] \tag{22}$$

where :

$$k_\psi(\psi_0) = \exp\left[f(\psi_0)/(f'(\psi_0)V_t)\right] \tag{23}$$

In Fig. 4 we show that Eq. 22 (surface) perfectly reproduces the numerically calculated band bending (circles) when both trapped and free charges are account for. As shown in the inset of Fig. 4, the percentage error between the numerical solution of Eq. 13 and its analytical approximation Eq. 22 is always below 0.1 %. It is worthwhile to note that Eq. 22 is a function of the physical and geometrical a-IGZO TFT parameters and of the band banding ψ_0 accounting for only the trapped charges, that reads [32]:

$$\psi_0 = V_G - V_{fb} - V_{ch} - 2V_t W_0\left[\frac{\sqrt{k_t}\epsilon_s}{2V_t C_i}e^{\frac{V_G - V_{fb} - V_{ch}}{2V_t}}\right] \tag{24}$$

where W_0 is the principal branch of the Lambert W function.

Unfortunately this function is not usually available in the most used CAD softwares or has to be implemented as an

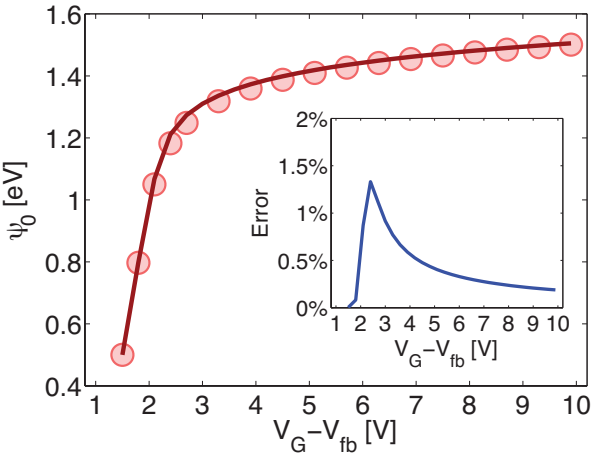

Fig. 5. Main Panel: Initial guess ψ_0 as a function of $V_G - V_{fb}$ at $V_{ch} = 1$V calculated by means of the Lambert function (circles) vs. the proposed approximation Eq. 27 (full line). Inset: Percentage error: $\|Eq.27 - Eq.24\|/Eq.24$. The physical parameters are listed in Tab. I.

internal function [33], therefore an analytical approximation is desirable. When the transistor works in linear region, i.e. $V_G - V_{fb} > V_{ch}$, the argument of W_0 grows very quickly thanks to its exponential dependence on $V_G - V_{fb} - V_{ch}$. A good approximation of W_0 in this regime is $W_0[x] = \log(x) - \log[\log(x)]$ [34] and it reads:

$$\psi_0 = 2V_t \log\left[\frac{2V_tC_i}{\sqrt{k_t}\epsilon_s}\log\left(\frac{\sqrt{k_t}\epsilon_s}{2V_tC_i}\right) + \frac{C_i(V_G - V_{fb} - V_{ch})}{\sqrt{k_t}\epsilon_s}\right] \quad (25)$$

On the other hand, in the subthreshold region, i.e. $V_G - V_{fb} < V_{ch}$, the argument of W_0 rapidly goes to zero and the band bending turns out to be:

$$\psi_0 = V_G - V_{fb} - V_{ch} \quad (26)$$

Eq. 25 and Eq. 26 are a very accurate approximation in the linear and subthreshold regions, respectively. In order to unify these two equations in a single continuous function we can combine them by means of the following function (Eq. 30 in [35]):

$$\log(1 + e^x) \simeq \begin{cases} x & \text{if } x > 0 \\ e^x & \text{if } x < 0 \end{cases}$$

and hence we obtain:

$$\psi_0 = 2V_t \log\left[\frac{2V_tC_i}{\sqrt{k_t}\epsilon_s}\log\left(1 + \frac{\sqrt{k_t}\epsilon_s}{2V_tC_i}e^{\frac{V_G - V_{fb} - V_{ch}}{2V_t}}\right)\right] \quad (27)$$

Eq. 27 is a continuous function that accurately approximates Eq. 24 in both the subthreshold and the linear regime (Fig. 5). As shown in the inset of Fig. 5, the maximum error is lower than 1.5%.

- If $V_G - V_{fb} - V_{ch} > 0$, Eq. 27 reduces to Eq. 25.
- If $V_G - V_{fb} - V_{ch} < 0$, Eq. 27 reduces to Eq. 26.

Eq. 22 with Eq. 27 is the analytical band bending model accounting for a double exponential function in Eq. 13, i.e. when both trapped and free charges are taken into account. In other words, for each value V_{ch} and V_G, Eq. 22 with Eq. 27 gives the band bending and, in turn, the surface potential, in each point of the channel.

IV. Fully Analytical Model

By means of the analytical band bending solution Eq. 22, the current model (Eq. 10) as a function of the applied voltages V_G, V_D, and V_S, reads:

$$I_D = [I_{dF}(\Phi_S) + I_{dT}(\Phi_S)] - [I_{dF}(\Phi_D) + I_{dT}(\Phi_D)] \quad (28)$$

where $\Phi_X = \sqrt{k_\psi(\psi_{0X})}(V_G - V_{fb} - V_X - \psi_{0X})$, $k_\psi(\psi_{0X})$ is defined in Eq. 23, $X \in \{S; D\}$, and ψ_{0S} and ψ_{0D} are the band bending calculated accounting for the trapped charge only (Eq. 27) at the source and the drain contact, respectively. I_{dF} and I_{dT}, in turn, can be reworked out as follows.

$$I_{dF}(\Phi_X) = \frac{W}{L}\beta\frac{\frac{k_f}{V_f}\left(\frac{\Phi_X}{\nu}\right)^{2\frac{T_t}{T}}}{\sqrt{A_F + B_F\left(\frac{\Phi_X}{\nu}\right)^{2-2\frac{T_t}{T}} + C_F\left(\frac{\Phi_X}{\nu}\right)^{4-4\frac{T_t}{T}}}} \quad (29)$$

$$I_{dT}(\Phi_X) = \frac{W}{L}\beta\frac{\frac{k_t}{V_t}\left(\frac{\Phi_X}{\nu}\right)^{2\frac{T_t}{T}}}{\sqrt{A_T\left(\frac{\Phi_X}{\nu}\right)^{4\frac{T_t}{T}-4} + B_T\left(\frac{\Phi_X}{\nu}\right)^{2\frac{T_t}{T}-2} + C_T}} \quad (30)$$

where $\nu = \epsilon_s\sqrt{k_t}/C_i$. Eqs. 28, 29, 30, 23, and 27 are the a-IGZO drain current model that accounts for both trapped and free charges. It is function of V_G,V_S, and V_D and TFT parameters.

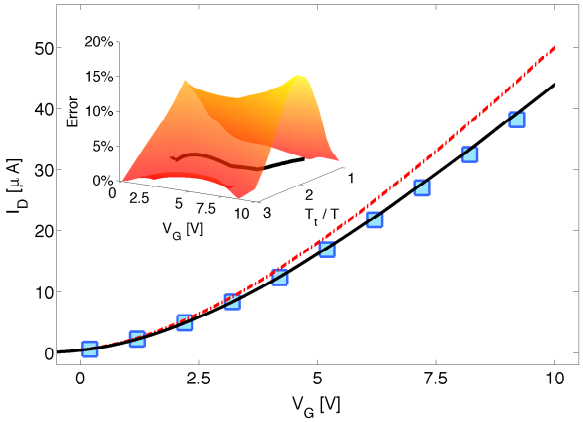

Fig. 6. Main Panel: Transfer characteristic of a-IGZO TFT at $V_D = 1$V. Squares are the numerical solution of Eq. 1, dashed line is the proposed analytical model (Eq. 28). Parameters are listed in Tab. I. The full line is the proposed analytical model (Eq. 28) with modified parameters: $N_f + 20\%$, and $\mu_0 - 15\%$. Inset: percentage error of the proposed analytical model with respect to the numerical solution of Eq. 1, using physical parameters listed in Tab. I (surface) and using modified parameters (for the analytical model only) for the maximum error case only (full line).

In order to assess the overall accuracy, the proposed fully analytical model is compared to the numerical solution of Eq. 1 in the inset of Fig. 6. The maximum percentage error is of 15 %. In all cases the analytical model overestimates the drain current. This is basically due to the approximation introduced in Eq. 6, that is required to obtain an analytical solution of Eq. 1.

We investigated the impact of the aforementioned approximation on the physical parameters returned by the analytical model. We have found that, for the maximum error case, this results in a 15% underestimation of μ_0 and in a 20%

TABLE I
GEOMETRICAL AND PHYSICAL PARAMETERS OF THE TRANSISTORS

W $[\mu m]$	1000	V_{fb} $[V]$	-2.87
L $[\mu m]$	100→5	N_t $[cm^{-3}]$	2.7 $\times 10^{19}$
k_s	7.9	N_f $[cm^{-3}]$	2.5 $\times 10^{20}$
C_i $[nF/cm^2]$	70	T_t $[K]$	523
μ_0 $[cm^2/Vs]$	11.8	T $[K]$	293

overestimation of N_f. It is worth noting that the former is comparable with the estimation accuracy of the field effect mobility and with the process variability, while the latter is negligible.

V. RESULTS AND DISCUSSION

The model is compared with the measurements of a-IGZO transistors [26] in a wide range of bias conditions. The physical parameters of the a-IGZO TFTs are extracted from the measured characteristics using the method proposed in [29]. It is worth noting that the TFT parameters are difficult to determine from the fabrication data because of the fabrication process variability and hence the TFT parameters have to be extracted from the electrical characteristics of several transistors. The estimation accuracy of the physical parameters N_t and N_f can be further improved by exploiting the analytical formulation of the model in a standard optimization problem. Physical and geometrical parameters are listed in Tab. I.

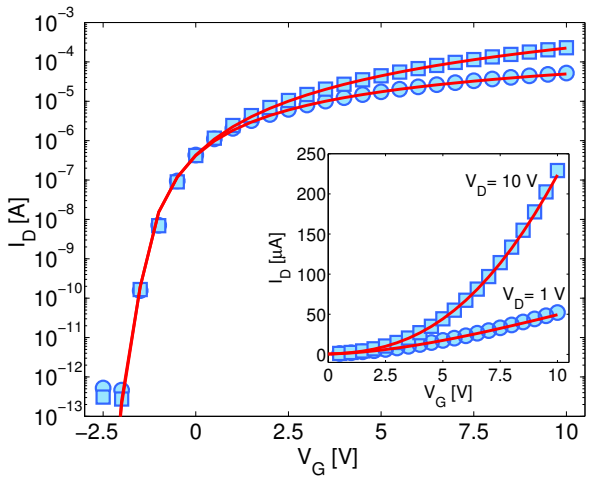

Fig. 7. Measured (symbols) and modeled (lines) transfer characteristics of L=100μm a-IGZO TFT. The transistor parameters are listed in Table I.

The comparisons between the measurements and the proposed analytical model are shown in Fig. 7. There is a very good agreement in the whole range of biasing conditions. In Fig. 8 the output characteristics are shown. In both the linear and the saturation region the model is in good agreement with the experimental data in the whole range of bias conditions. Finally, in Fig. 9 the L/W normalized current, of transistors with channel length ranging from $5\mu m$ to $100\mu m$ are shown. A very good agreement between the model and the measured data is achieved in the linear region. At large drain voltages (saturation region) the model overestimates the drain current with a maximum error of 2%: it is due to the contact effects [26][36][37] which are not included in this model.

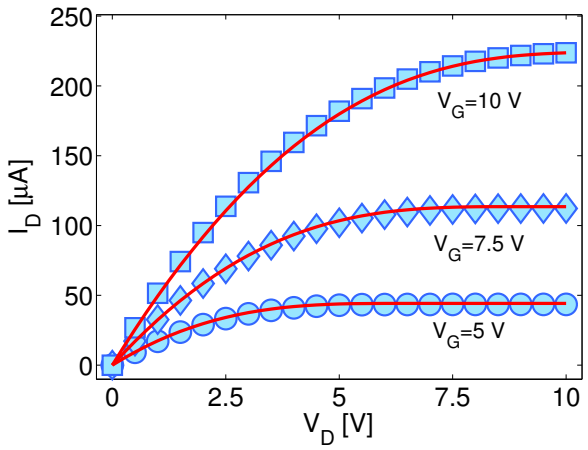

Fig. 8. Measured (symbols) and modeled (lines) output characteristics of L=100μm a-IGZO TFT. The transistor parameters are listed in Table I.

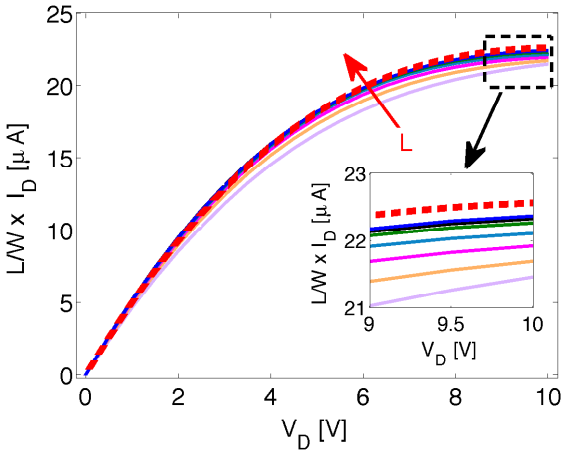

Fig. 9. Measured (full lines) and modeled (dashed line) L/W normalized output characteristics of a-IGZO TFTs at $V_G = 10$V. Geometrical and physical parameters are listed in Tab. I.

VI. CONCLUSION

A physical based analytical model for a-IGZO TFTs is proposed. Both trap-limited conduction and percolation in the conduction band are included. The model accurately reproduces the measurements of a-IGZO TFTs fabricated on flexible substrate. Thanks to its analytical and simple formulation it can be used in a CAD software for the design of high-functionality circuits, for the physical parameters extraction and for the process characterization.

REFERENCES

[1] K. Nomura, H. Ohta, A. Takagi, T. Kamiya, M. Hirano, and H. Hosono, "Room-temperature fabrication of transparent flexible thin-film transistors using amorphous oxide semiconductors," *Nature*, vol. 432, no. 7016, pp. 488-492, Nov. 2004.

[2] R. A. Street, T. N. Ng, R. A. Lujan, I. Son, M. Smith, S. Kim, T. Lee, Y. Moon, and S. Cho, "Sol-Gel Solution-Deposited InGaZnO Thin Film Transistors," *ACS Appl. Mater. Inter.*, vol. 6, no. 6, pp. 4428-4437, Mar. 2014.

[3] G. H. Kim, H. S. Kim, H. S. Shin, B. D. Ahn, K. H. Kim, and H. J. Kim, "Inkjet-printed InGaZnO thin film transistor," *Thin Solid Films*, vol. 517, no. 14, pp. 4007-4010, May. 2009.

[4] T. Kamiya, K. Nomura, and H. Hosono, "Present status of amorphous In-Ga-Zn-O thin-film transistors," *Sci. Technol. Adv. Mater.*, vol. 11, no. 4, pp. 044305, Aug. 2010.

[5] D.J. Yang, G.C. Whitfield, N.G. Cho, P.-S. Cho, I.-D. Kim, H.M. Saltsburg, and H.L. Tuller, "Amorphous $InGaZnO_4$ films: gas sensor response and stability," *Sens. Actuators, B*, vol. 171-172, pp. 1166-1171, Aug. 2012.

[6] J. T. Smith, S. S. Shah, M. Goryll, J. R. Stowell, and D. R. Allee, "Flexible ISFET Biosensor Using IGZO Metal Oxide TFTs and an ITO Sensing Layer," *IEEE Sensors Journal*, vol. 14, no. 4, pp. 937-938, Apr. 2014.

[7] M. C. Chen, T. C. Chang, S. Y. Huang, S. C. Chen, C. W. Hu, C. T. Tsai, and S. M. Sze, "Bipolar resistive switching characteristics of transparent indium gallium zinc oxide resistive random access memory," *Electrochem. Solid State Lett.*, vol. 13, no. 6, pp. H191-H193, Mar. 2010.

[8] A. K. Tripathi, E. C. P Smits, J. B. P. H. van der Putten, M.van Neer, K. Myny, M. Nag, S. Steudel, P. Vicca, K. O'Neill, E. van Veenendaal, J. Genoe, P. Heremans, and G.H. Gelinck, "Low-voltage gallium-indium-zinc-oxide thin film transistors based logic circuits on thin plastic foil: Building blocks for radio frequency identification application," *Appl. Phys. Lett.*, vol. 98, no. 16, pp. 162102-1-162102-3, Apr. 2011.

[9] D. Raiteri, F. Torricelli, K. Myny, M. Nag, B. Van Der Putten, E. Smits, S. Steudel, K. Tempelaars, A. Tripathi, G. Gelinck, A. Van Roermund, and E. Cantatore, "A 6b 10MS/s current-steering DAC manufactured with amorphous Gallium-Indium-Zinc-Oxide TFTs achieving SFDR $>$ 30dB up to 300kHz," *ISSCC Dig. Tech. Pap. I.*, vol. 55, pp. 314-315, Feb. 2012.

[10] T. Kamiya, K. Nomura, and H. Hosono, "Electronic Structures Above Mobility Edges in Crystalline and Amorphous In-Ga-Zn-O: Percolation Conduction Examined by Analytical Model," *J. Display Technol.*, vol. 5, no. 12, pp. 462-467, Dec. 2009.

[11] K. Nomura, T. Kamiya, H. Ohta, K. Ueda, M. Hirano, and H. Hosono, "Carrier transport in transparent oxide semiconductor with intrinsic structural randomness probed using single-crystalline $InGaO_3(ZnO)_5$ films," *Appl. Phys. Lett.*, vol. 85, no. 11, pp. 1993-1995, Sep. 2004.

[12] W. Körner, D. F. Urban, C. and Elsässer, "Origin of subgap states in amorphous In-Ga-Zn-O," *J. Appl. Phys.*, vol. 114, no. 16, pp. 163704-1-163704-6, Oct. 2013.

[13] H. Hsieh, T. Kamiya, K. Nomura, H. Hosono, and C. Wu, "Modeling of amorphous $InGaZnO_4$ thin film transistors and their subgap density of states," *Appl. Phys. Lett.*, vol. 92, no. 13, pp. 133503, Apr. 2008.

[14] J. K. Jeong, J. H. Jeong, H. W. Yang, J.-S. Park, Y.-G. Mo, and H. D. Kim, "High performance thin film transistors with cosputtered amorphous indium gallium zinc oxide channel," *Appl. Phys. Lett.*, vol. 91, no. 11, pp. 113505-1-113505-3, Sep. 2007.

[15] C-G. Lee, B. Cobb, and A. Dodabalapur, "Band transport and mobility edge in amorphous solution-processed zinc tin oxide thin-film transistors," *Appl. Phys. Lett.*, vol. 97, no. 20, pp. 203505-1-203505-3, Nov. 2010.

[16] S. Lee, K. Ghaffarzadeh, A. Nathan, J. Robertson, S. Jeon, C. Kim, I-H. Song, and U-I. Chung, "Trap-limited and percolation conduction mechanisms in amorphous oxide semiconductor thin film transistors," *Appl. Phys. Lett.*, vol. 98, no. 20, pp. 203508-1-203508-3, Mag. 2011.

[17] J. Jeong, J. K. Jeong, J.-S. Park, Y.-G. Mo, and Y. Hong, "Meyer-Neldel Rule and Extraction of Density of States in Amorphous Indium-Gallium-Zinc-Oxide Thin-Film Transistor by Considering Surface Band Bending," *Jpn. J. Appl. Phys.*, vol. 49, no. 3S, pp. 03CB02-1-03CB02-6, Mar. 2010.

[18] K. Jeon, C. Kim, I. Song, J. Park, S. Kim, S. Kim, Y. Park, J.-H. Park, S. Lee, D. M. Kim, and D. H. Kim, "Modeling of amorphous InGaZnO thin-film transistors based on the density of states extracted from the optical response of capacitance-voltage characteristics," *Appl. Phys. Lett.*, vol. 93, no. 18, pp. 182102-1-182102-3, Nov. 2008.

[19] Y. W. Jeon, S. Kim, S. Lee, D. M. Kim, D. H. Kim, J. Park, C. J. Kim, I. Song, Y. Park, U-I. Chung, J.-H. Lee, B. D. Ahn, S. Y. Park, J.-H. Park, and J. H. Kim, "Subgap Density-of-States-Based Amorphous Oxide Thin Film Transistor Simulator (DeAOTS)," *IEEE Trans. Electron Devices*, vol. 57, no. 11, pp. 2988-3000, Nov. 2010.

[20] S. Lee, S. Park, S. Kim, Y. Jeon, K. Jeon, J.-H. Park, J. Park, I. Song, C. J. Kim, Y. Park, D. M. Kim, and D. H. Kim, "Extraction of Subgap Density of States in Amorphous InGaZnO Thin-Film Transistors by Using Multifrequency Capacitance-Voltage Characteristics," *IEEE Electron Device Lett.*, vol. 31, no. 3, pp. 231-233, Mar. 2010.

[21] Y. Kim, M. Bae, W. Kim, D. Kong, H. K. Jeong, H. Kim, S. Choi, D. M. Kim, and D. H. Kim, "Amorphous InGaZnO Thin-Film Transistors - Part I: Complete Extraction of Density of States Over the Full Subband-Gap Energy Range," *IEEE Trans. Electron Devices*, vol. 59, no. 10, pp. 2689-2698, Oct. 2012.

[22] S. Y. Lee, D. H. Kim, E. Chong, Y. W. Jeon, and D. H. Kim, "Effect of channel thickness on density of states in amorphous InGaZnO thin film transistor," *Appl. Phys. Lett.*, vol. 98, no. 12, pp. 122105, Mar. 2011.

[23] T.-C. Fung, C.-S. Chuang, C. Chen, K. Abe, R. Cottle, M. Townsend, H. Kumomi, and J. Kanicki, "Two-dimensional numerical simulation of radio frequency sputter amorphous InGaZnO thin-film transistors," *J. Appl. Phys.* vol. 106, no. 8, pp. 084511-1-084511-10, Oct. 2009.

[24] A. Tsormpatzoglou, N. A. Hastas, N. Choi, F. Mahmoudabadi, M. K. Hatalis, and C. A. Dimitriadis, "Analytical surface-potential-based drain current model for amorphous InGaZnO thin film transistors," *J. Appl. Phys.*, vol. 114, no. 18, pp. 184502-1-184502-6, Nov. 2013.

[25] C. Perumal, K. Ishida, R. Shabanpour, B. K. Boroujeni, L. Petti, N. S. Münzenrieder, G. A. Salvatore, C. Carta, G. Tröster, and F. Ellinger, "A Compact a-IGZO TFT Model Based on MOSFET SPICE Level = 3 Template for Analog/RF Circuit Designs," *IEEE Electron Device Lett.*, vol. 34, no. 11, pp. 1391-1393, Nov. 2013.

[26] F. Torricelli, A. K. Tripathi, E. C. P. Smits, L. Colalongo, Z. M. Kovacs-Vajna, G. H. Gelinck, and E. Cantatore, "Analysis and Modeling of Amorphous InGaZnO (aIGZO) Thin-Film Transistors," *14th Workshop on Semiconductor Advances for Future Electronics*, Veldhoven, The Netherlands, Nov. 2011.

[27] A. Cerdeira, M. Estrada, B.S. Soto-Cruz , B. Iñiguez, "Modeling the behavior of amorphous oxide thin film transistors before and after bias stress," *Microeltron. Reliab.*, vol. 52, no. 11, pp. 2532-2536, Nov. 2012.

[28] F. Torricelli, J. R. Meijboom, E. C. P. Smits, A. K. Tripathi, M. Ferroni, S. Federici, G. H. Gelinck, L. Colalongo, Z. M. Kovacs-Vajna, D. M. de Leeuw, and E. Cantatore,"Transport Physics and Device Modeling of Zinc Oxide Thin-Film Transistors - Part I: Long-Channel Devices," *IEEE Trans. Electr. Devices*, vol. 58, no. 8, pp. 2610-2619, Aug. 2011.

[29] F. Torricelli, K. O'Neill, G. H. Gelinck, K. Myny, J. Genoe, and E. Cantatore, "Charge Transport in Organic Transistors Accounting for a Wide Distribution of Carrier Energies - Part II: TFT Modeling," *IEEE Trans. Electron Devices*, vol. 59, no. 5, pp. 1520-1528, May 2012.

[30] L. Colalongo, "A new analytical model for amorphous-silicon thin-film transistors including tail and deep states," *Solid-State Electron.*, vol. 45, no. 9, pp. 1525-1530, Sep. 2001.

[31] S. Lee, and A. Nathan, "Localized tail state distribution in amorphous oxide transistors deduced from low temperature measurements" *Appl. Phys. Lett.*, vol. 101, no. 11, pp. 113502-1-113502-5, Sep. 2012.

[32] F. J. García-Sánchez, and A. Ortiz-Conde, "An Explicit Analytic Compact Model for Nanocrystalline Zinc Oxide Thin-Film Transistors," *IEEE Trans. Electron Devices*, vol. 59, no. 1, pp. 46-50, Jan. 2012.

[33] J. Alvarado, B. Iñiguez, M. Estrada, D. Flandre, and A. Cerdeira, "Implementation of the symmetric doped double-gate MOSFET model in Verilog-A for circuit simulation," *Int. J. Numer. Model.*, vol. 23, no. 2, pp. 88-106, Mar./Apr. 2010.

[34] A. Hoorfar, and H. Mehdi, "Inequalities on the Lambert W function and hyperpower function," *J. Inequal. Pure and Appl. Mathematics* vol. 9, no. 2, pp. 51-1-51-5, Mar. 2008.

[35] C. C. Enz, F. Krummenacher, and E.A. Vittoz, "An Analytical MOS Transistor Model Valid in All Regions of Operation and Dedicated to Low-Voltage and Low-Current Applications," *Analog Integrated Circuits and Processing*, vol. 8, no. 1, pp. 83-114, Jul. 1995.

[36] J. Park, C. Kim, S. Kim, I. Song, S. Kim, D. Kang, H. Lim, H. Yin, R. Jung, E. Lee, J. Lee, K.-W. Kwon, and Y. Park, "Source/Drain Series-Resistance Effects in Amorphous Gallium-Indium Zinc-Oxide Thin Film Transistors," *IEEE Electr. Device Lett.*, vol. 29, no. 8, pp. 879-881, Aug. 2008.

[37] F. Torricelli, E. C. P. Smits, J. R. Meijboom, A. K. Tripathi, G. H. Gelinck, L. Colalongo, Z. M. Kovacs-Vajna, D. M. de Leeuw, and E. Cantatore,"Transport Physics and Device Modeling of Zinc Oxide Thin-Film Transistors - Part II: Contact Resistance in Short-Channel Devices," *IEEE Trans. Electr. Devices*, vol. 58, no. 9, pp. 3025-3033, Sep. 2011.